# Fluorescent imaging system for global measurement of liquid film thickness and dynamic contact angle in free surface flows

Cite as: Review of Scientific Instruments **68**, 4097 (1997); https://doi.org/10.1063/1.1148352
Submitted: 22 April 1997 • Accepted: 15 July 1997 • Published Online: 04 June 1998

**M. F. G. Johnson, R. A. Schluter and S. G. Bankoff**



# Fluorescent imaging system for global measurement of liquid film thickness and dynamic contact angle in free surface flows

M. F. G. Johnson
*Department of Mechanical Engineering, Northwestern University, Evanston, Illinois 60208-3120*

R. A. Schluter
*Department of Physics and Astronomy, Northwestern University, Evanston, Illinois 60208-3120*

S. G. Bankoff[a)]
*Department of Chemical Engineering, Northwestern University, Evanston, Illinois 60208-3120*

(Received 22 April 1997; accepted for publication 15 July 1997)

Fluorescent dye dissolved in a liquid flow was used to outline liquid-gas free boundaries and, with digital imaging, to observe quantitatively surface wave propagation and pattern formation, as well as contact-line velocity and contact angle in thin film flows on horizontal and inclined substrates. Using the relatively inexpensive system described here, a fluid depth measurement with a precision of $\pm 0.02$ mm is obtained routinely in flows of several millimeters depth over an area of approximately one square meter, and essentially unlimited continuous time spans. Dynamic contact angles are measured, for the first time, on liquid fronts with significant three-dimensional curvature such as rivulets draining down an inclined plate at any speed or global location. Procedures to normalize results quantitatively for any nonuniformities of the incident illumination are given. Estimates of the contribution to the experimental error by other effects, such as variations in dye concentration and temperature, and image digital register capacity, are also discussed. Illustrative results for two fluids and several dyes are given. Refinements to decrease the local error further to $\pm 0.005$ mm or less are described. © *1997 American Institute of Physics.*
[S0034-6748(97)00311-0]

## I. INTRODUCTION

This article describes a method for experimentally defining the dynamic surface of a thin liquid flowing film. The general problem is an old one, both in experiment and in associated theory. Experimental methods developed previously for the measurement of a free surface flow are described in recent reviews by Goldstein,[1] Cha and Trolinger,[2] Yang,[3] and Alekseenko *et al.*[4] Recent results for the case of surface waves on a continuous flow using fluorescent delineation of patterns have been obtained by Liu *et al.*[5] and Knaani *et al.*[6] This article details the quantitative development of the method of fluorescent imaging for the study of continuous films and the movement of a fluid front along a solid surface. The method is also applied, for the first time, to the global measurement of the dynamic contact for a fluid front advancing at velocities of the order of millimeters per second and greater.

Our method produces results germane to several broad areas of theoretical hydrodynamics which have been active for many decades, and toward which we have applied the method described in this article: (i) wave phenomena on a continuous film, both isothermal and temperature driven, current theory reviewed by Oron *et al.*,[7] Joo *et al.*,[8] Liu *et al.*,[5] and Chang;[9] (ii) fluid rupture behavior (dry spot formation) and microscopic contact angle (definition) current theory reviewed by de Gennes;[10] (iii) rivulet instability and rivulet shape, reviewed by Hocking and Miksis[11] and Lopez *et al.*[12,13]

a)Corresponding author; Electronic mail: gbankoff@casbah.acns.nwu.edu

## II. METHOD

A broad source of near-ultraviolet (UV) light illuminates a thin fluid film such that each volume element in the fluid receives approximately equal incident light energy per unit volume. A relatively small concentration of a fluorescent solute produces a characteristic emission band, which is sighted along a line nearly perpendicular to the fluid surface into the receiving charge coupled device (CCD) camera. A filter narrows the receptivity of the camera to the emission color of the fluorescent solute, and another large area filter over the UV bulb bank removes traces of spurious light to which the camera is sensitive from the incident UV of the fluorescent color. The camera produces a time series of digital images in which the pixel amplitude is a linear representation of the amount of fluorescent solute in the sightline of the camera. Experimental images of a flow field are corrected for true fluid depth and for velocity using a calibration image which are recorded for similar conditions as the experimental image. Analytic procedures are then performed on an image file to obtain fluid flow quantities such as depth, fluid surface gradient, contact line shape, and contact line velocity. The method does not reveal internal fluid velocities, except when small bubbles are present, a potentiality observed but not pursued in the present work. The essential features of the optical geometry at the fluid surface are diagrammed in Fig. 1. The accuracy of the method depends on these points:

(1) The UV light is nearly uniform spatially, of nearly hemispherical incidence in angle, and can furthermore is accurately normalized spatially for each run (Sec. IV).

(2) The fluorescent dye is uniformly distributed throughout the fluid and cannot change in concentration during op-

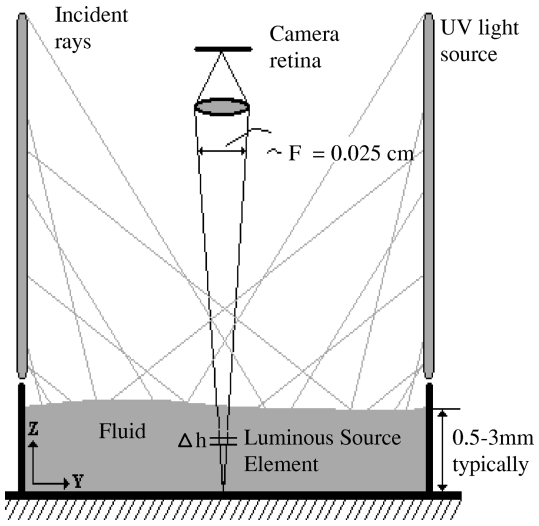


FIG. 1. Fluorescent imaging system used to measure fluid depth at any time and point in the flow field.

eration and the luminance intensity, therefore the depth, is proportional to the absolute amount of fluorescein in the line of sight of the camera, adjusted for absorption in the fluid (Sec. IV).

(3) The amplitude response of the CCD camera, as well as all stages up to the analog/digital signal conversion, is linear.

(4) The effects of optical resolution on the stored experimental image is understood and can be corrected where needed, as detailed in Sec. V.

## III. FLUORESCENT IMAGING SYSTEM

Two banks of standard forty inch UV bulbs[14] flank the camera facing the fluid substrate surface of area up to 0.8 m×0.97 m. The entire frame carrying bulbs, camera, and fluid flow system, shown in Fig. 2, can be inclined at angles from 0° to 40°. A separate but similar system is used for fluid flow on a vertical surface. The substrate does not have to be transparent as it must be for methods which use transmitted light to measure fluid depths. Two plastic filters are used to remove light of undesirable wavelengths, with the combined effect shown in Fig. 3. The bulb planes are covered by a plastic filter to remove a slight component in the visible,[15] and the camera lens has a plastic filter bracketing the fluorescent emission.[16] The substrates vary according to desired fluid–solid interface characteristics, but are always black.

One of two lenses, a Fujinon TV zoom lens, 16–160 mm and maximum aperture of $f/1.8$, typically $f/4$, or a higher resolution Bolex-Lytar, 25 mm lens is mounted on a Sony XC-75 CCD camera. The Fujinon lens permits changing of fluid space viewing area from about $2\times3$ cm$^2$ to $50\times70$ cm$^2$ in the present frame. The video board[17] with an image analysis software package,[18] is capable of storing 13 images with a time interval of 0.33 s or unlimited frames (dependent on available disk storage) at an interval of 0.50 s. This feature is used to obtain velocities of surface waves and of contact lines.

Pixel location in the fluid space is calibrated by recording a scale and counting the number of pixels corresponding to that length. Distortion is negligible; the error interval (symmetric) in measured coordinates in the plane of the fluid is due to pixel size, and varies from about 1.5 mm for a viewing dimension of 70 cm to 0.06 mm for a viewing dimension of 3 cm.

Although not strictly a feature of the measurement method, we mention the precautions found necessary to avoid spurious disturbances in the highly sensitive fluid flow, typically a millimeter in depth and a flow area to 0.8 m×0.97 m. The edge(s) defining the flow must be free of deviation to about 0.01% of the flow depth; otherwise, easily visible noise occurs immediately in the flow. In fact, the edge deviations are removed by careful localized lapping of the edge (glass or metal), using the spurious agitation as an indicator. Also, the flow is very sensitive to vibration; noise at the level of normal conversation produces visible excitation. Therefore, the pulsing of the metering gear pump is carefully damped by free surface volume and resistance through a flow filter. The frame holding the entire system, fluid, plane, and optics, is tied to the concrete frame of the building at several points, which leaves micro-oscillations of the building as a vibration base level. In some experiments without imposed wave stimulation we have found a longer period of flow before ''spontaneous'' oscillations appear if we run the system in the early morning when ambient traffic is less.

## IV. FLUID DEPTH CALIBRATION

Converting the pixel intensity (an electronic amplitude) to a physical depth requires a physical calibration under the

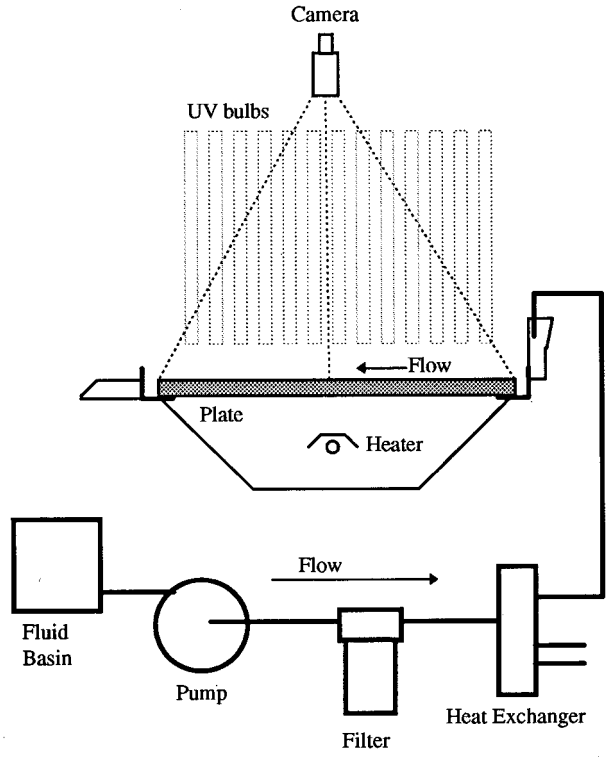


FIG. 2. Experimental facility showing fluid flow and optical systems.

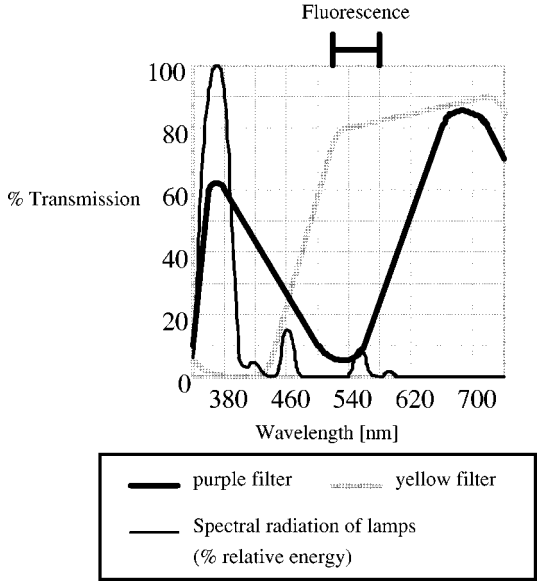


FIG. 3. Transmission curves for yellow and purple filters and spectral radiation of UV lamps.

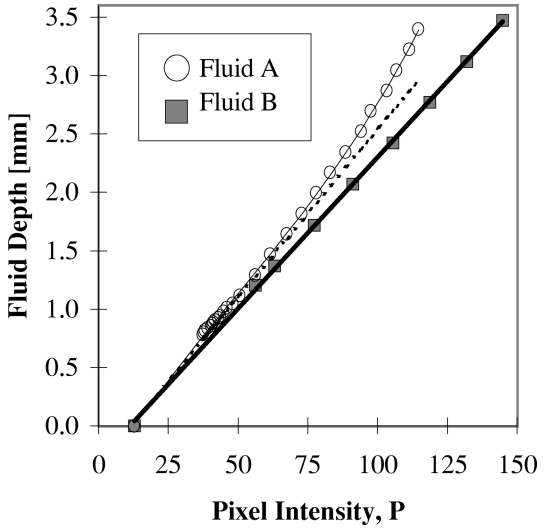


FIG. 5. Calibration curve for converting pixel intensity or gray scale values from the imaging system to actual fluid depth values. The actual data are shown together with curves fitted according to Eq. (2). The dotted line represents a straight-line extrapolation.

exact conditions of a given fluid flow run. The relatively small variation in UV light intensity is accounted for by taking 20 or more frames under the investigated flow conditions, and taking the average of these frames extending over several seconds or a shorter time scale when compared with the gross motion of the fluid. The resulting average is, and is required to be, structureless, therefore representing the local average flow conditions. The resulting average image is done for any experimental record. The variation of UV illumination intensity shown is typically 15% with the broad source bank in use, as shown in Fig. 4 for surface waves on a continuous fluid film. The experimental pixel intensities are then normalized using this time-averaged image.

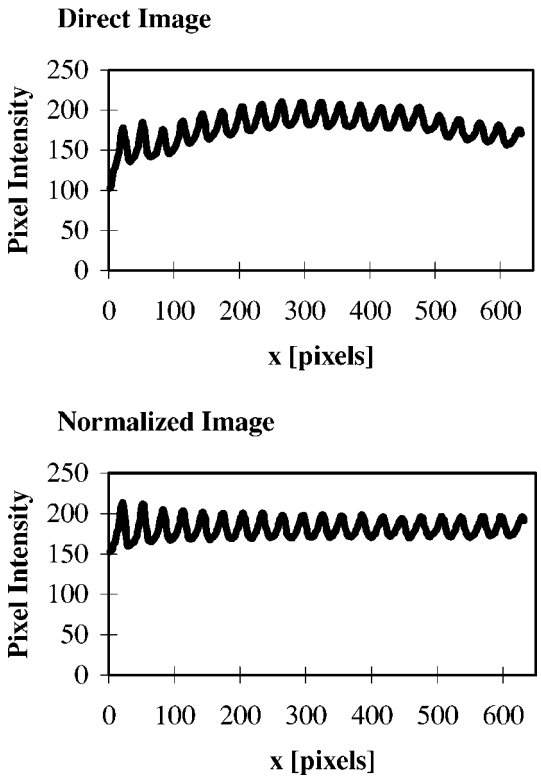


FIG. 4. Plots of centerline depth profile for a continuous film showing lighting effects for a regular image and a normalized image.

The relation of actual depth to pixel intensity is obtained by putting a small pool of the experimental fluid into the illuminated space and increasing the depth by precise volumetric increments. Two typical calibration curves for two fluid mixtures composed of different percentages of water and glycerin (fluid A and fluid B, with weight percents of glycerin to water of 68% and 77%, respectively) are shown in Fig. 5. Note that the signal goes to a zero value at zero depth; there is no residual fluorescent film at zero fluid depth. The proportionality of pixel amplitude to total amount of fluorescent solute in the sight line was further checked by successive dilution with distilled water of a fixed sample and finding no change, to within 1%. Figure 5, shows a slight nonlinearity of response for fluid A. Taking into account self-absorption, both of incoming UV and outgoing fluorescence, and assuming a perfectly absorbing background, one expects the light intensity into a pixel, $P$, in the lens to follow:

TABLE I. Measured fluid depths ($d_{om}$) and calculated depth ($d_o$) for a continuous film.

| $\beta$ [degrees] | Re [−] | $d_{om}$ [mm] | $d_o$ [mm] |
|---|---|---|---|
| 23.3 | 0.6 | 0.80 | 0.74 |
| 23.3 | 2.4 | 1.24 | 1.17 |
| 23.3 | 4.6 | 1.50 | 1.46 |
| 14.5 | 0.6 | 0.92 | 0.86 |
| 14.5 | 2.4 | 1.45 | 1.37 |
| 14.5 | 4.6 | 1.79 | 1.70 |
| 6.0 | 0.6 | 1.26 | 1.15 |
| 6.0 | 2.4 | 1.92 | 1.83 |
| 6.0 | 4.6 | 2.34 | 2.27 |

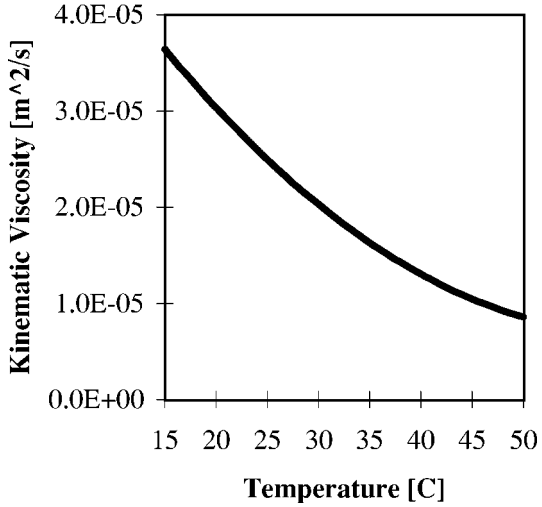


FIG. 6. Temperature dependent curves for kinematic viscosity for fluid A.

$$\frac{\partial P}{\partial h} = \kappa e^{-\alpha h} \tag{1}$$

which yields:

$$P = \kappa h - \kappa\alpha \frac{h^2}{2} + \kappa \frac{\alpha^2 h^3}{6} \tag{2}$$

which is an approximation to the curves of Fig. 5, where $\kappa$ contains the luminous emission efficiency of the fluorescent solute and the incident UV illumination intensity, as well as the camera lens $f$/stop and the entire electronic and digital conversion transfer factor. The term $\alpha$ in Eq. (2) is an inverse absorption length, and represents the self-absorption of both UV and fluorescent emission in the fluid. It is actually the sum of these absorption lengths. It is important to note that all these factors are present in the normalizing run and in the static calibration run, and are removed by our normalization procedure. Fitting curves according to Eq. (2) to the data as in Fig. 5, leads to an average absorption length of 12.6 $\pm$ 0.6 mm which compares well with a direct-transmission experiment, which yielded $11.5 \pm 1.0$ mm for fluid A. The curve for fluid B gives a larger value for the absorption length, and thus does not significantly vary from a linear value over the range of fluid depths tested.

The calibration method was checked by measuring the fluid depth of a continuous flow down an inclined plane at different flowrates and angles of inclination of the plate. This fluid depth ($d_{om}$) is compared to the values of the fluid depth ($d_o$) calculated using the Nusselt equation:

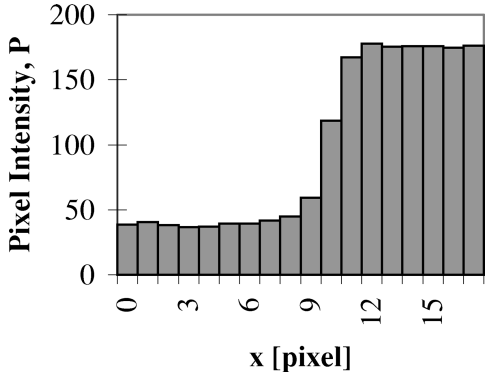


FIG. 7. Pixel intensity variation across a sharp transition from a low to high intensity region. One pixel width is ~0.23 mm in fluid space.

$$d_o = [3Q\nu/g \sin\beta]^{1/3}, \tag{3}$$

where $Q$ is the volumetric flowrate per unit width of the plate, $\nu$ is the kinematic viscosity, $g$ is the gravitational constant, and $\beta$ is the plate angle of inclination. The values for $d_{om}$ and $d_o$ are given in Table I, which show that the measured values compare well with the calculated values, with the value of $d_{om}$ being consistently larger than $d_o$ by an average of 5%. The difference can be attributed to small surface waves which dissipate energy, so that the measured depth would be larger than the calculated value.

We have used mainly fluorescein[19] in various glycerin/water mixtures for which Fig. 6 shows the range as a function of temperature for the kinematic viscosity for one of the mixtures. Table II shows the results of a survey of several dyes with several solvents, compared on a relative scale to fluorescein/water/glycerin. Included is canola oil, which is furthermore self-fluorescent and sufficiently transparent to be of use in this method.

## V. CONTACT ANGLE

Dynamic contact angles are difficult to measure, except at slow contact line speeds and with straight contact lines, where side silhouette photography has been successfully used. Deflection of a light beam at a fixed location has also

TABLE II. Pixel intensity of solutions with different dyes for a fluid depth of 4.3 mm.

| | Glycerol, 99+% | Water (distilled) | Ethyl alcohol | Light mineral oil | Canola oil | Silicone oil |
|---|---|---|---|---|---|---|
| Fluorescein | 42 | 100 | 95 | 15 | 20 | 20 |
| 4′,5′-dibromofluorescein | 38 | 25 | 58 | | | |
| 2′,7′-dichlorofluorescein | 67 | 89 | 234 | | | |
| Acridine orange | 96 | 14 | 128 | | | |
| Xylenol orange | 27 | 12 | 13 | | | |
| Nile blue a | 14 | 12 | 14 | | | |
| Fluorescein diacetate | 16 | 20 | 70 | | | |
| Rhodamine 6g | 138 | 21 | 247 | | | |
| Bis(phenylethynyl) Anthracene [ $f$-stop = 5.6] | 17 | 18 | 111 | 170 | 167 | 44 |

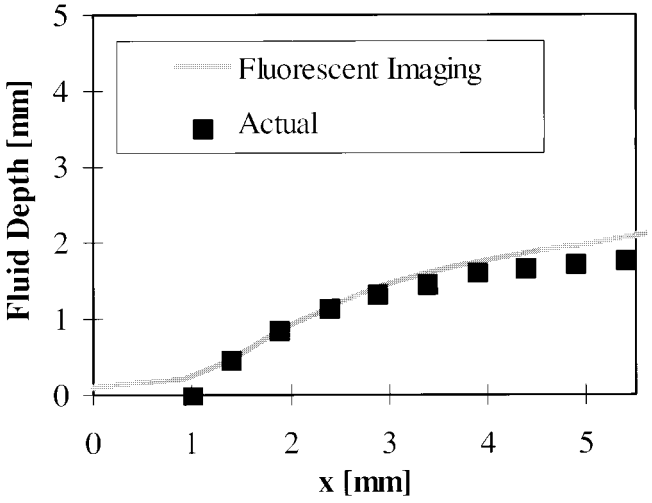


FIG. 8. Comparison of fluid depth measured using fluorescent imaging method with actual values along the interface of a fluid drop.

been used, but is subject to error if the advancing front has significant three-dimensional curvature and is limited to measuring at one point in the flow field. The fluorescent imaging method described here can be used to measure contact angles on a three-dimensional front, such as a liquid finger protruding from a liquid sheet advancing down an inclined plane, to within $\pm 1°$ at any contact line speed, and follow the development of the contact angle globally in space and time.

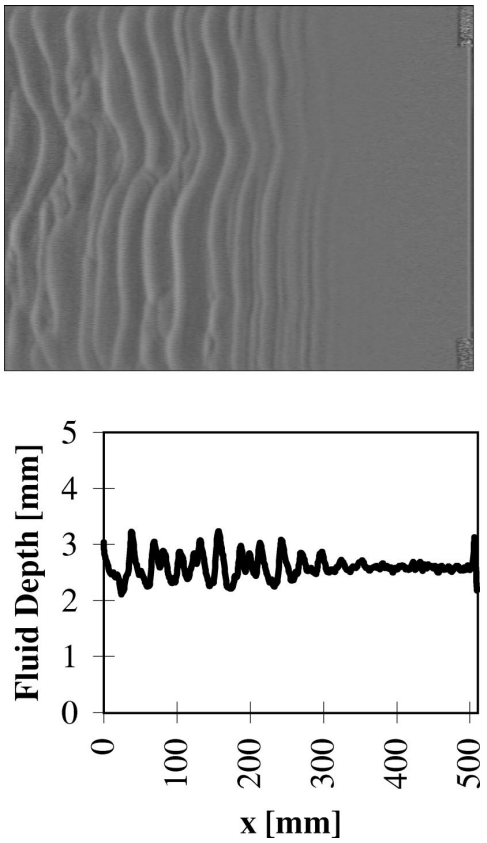


FIG. 9. Flow image and centerline depth profile for a thin film of water/glycerin mixture at an angle of inclination of 19.7°, Re = 11.63, isothermal and unperturbed condition. Flow direction is from right to left.

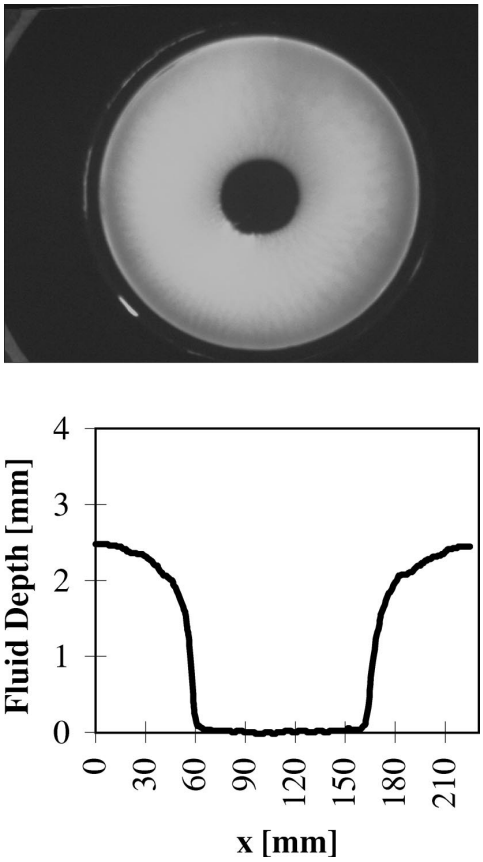


FIG. 10. Flow image and centerline depth profile for the formation of a dry spot from a thin heated film of ethyl alcohol.

There are two critical aspects of the measurements: the detailed physical situation at the contact vertex, which brings in the effective optical resolution of the system, and an optical enhancement effect springing from additional UV light capture approximately proportional to the slope of the fluid surface. Both effects have been studied.

The measurement of fluid boundary shape and fluid depth behind a contact line does not depend critically on optical resolution. However, detail at the contact line vertex is limited by three effects: (1) optical resolution of the lens, (2) light scattering (lack of contrast) in the lens, and (3) digital camera pixel size. In order to determine the size of a region in which a change of slope of the fluid as it approaches the contact line would be obscured by limited resolution, a boundary of a bright strip on the dark substrate background was recorded under typical magnification, as shown in Fig. 7. The pixel size (projecting to 200 $\mu$m in fluid space) is seen to be the limiting condition in our apparatus. This effect determines the limit on the detection of a physical precursor, or ''foot,'' as has sometimes been hypothesized, to a physical region of the order of the pixel size projecting by optical magnification into the fluid space. Figure 7 shows a contact line observation for which the resolution is approximately two pixels.

Under conditions where the fluid free surface boundary is not parallel to the substrate, as would be the case in an advancing fluid front, a correction for surface inclination is considered. A surface with a contact angle of $\theta_s$ has a UV light flux component parallel to the substrate. The intensity

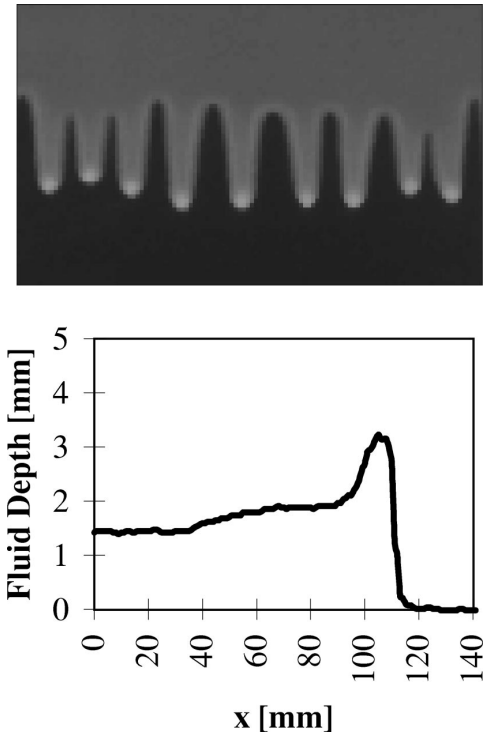


FIG. 11. Flow image and centerline depth profile for the formation of rivulets from a water/glycerin mixture at an angle of inclination of 14.5°, Re = 4.6. Flow direction is from top to bottom.

contributed by this component is proportional to the brightness of the UV normal to the sloped fluid face and to $\theta_s$, approximately, for small $\theta_s$. We have measured flat prisms of fluorescent fluid with specified end face inclinations in our standard experimental conditions and the resulting recorded images are in agreement with this model, with the further result that the absorption of the parallel UV light is consistent with the absorption length of 12 mm found in direct measurement.[20] This effect is negligible for cases where the contact angle is $<20°$ as shown in Fig. 8 for a drop of fluid A on a glass surface, $\theta_s = 17°$. The fluid shape found using the fluorescent imaging method agrees with the actual shape, which is measured by tracing the outline of the drop using a traveling microscope. Examples given in Sec. VII also have a correction of 5%, or less, due to the UV intensity effect described.

## VI. EXPERIMENTAL ERROR

The experimental error represented in, e.g., Fig. 5 is dominated by (1) statistical fluctuations in the pixel signal buffers (content 255) in our image capture card. Other factors, all systematic, are: (2) consistency of fluorescent dye density in time and among calibration measurements, (3) constancy of UV source conditions, (4) constancy of the video signals from charge capture in the CCD camera, through electronic amplification, to A/D conversion. An order of magnitude improvement in (1) would be easily attainable, yielding an error in the range $\pm 0.005$ mm.

## VII. ILLUSTRATIVE RESULTS

We show three examples of the use of the fluorescent imaging method for measuring fluid depth values. (i) Figure 9 shows the flow image and the measured centerline depth profile for a thin film of water/glycerin mixture on an inclined plate at an angle of 19.7°, Reynolds number = 11.63, showing developing spontaneous wave disturbances.[5–8] (ii) Figure 10, shows a rupture in a thin film under heat stress, and the measured depth cross-section profile. (iii) Figure 11 shows the fluorescent image and a measured profile down the mid-line of a developing rivulet finger.[10,11]

## ACKNOWLEDGMENTS

This work was supported by the Division of Basic Energy Sciences, Department of Energy, the National Science Foundation and by the NASA Graduate Student Researcher Program. M. J. Miksis is thanked for his helpful comments.

[1] R. J. Goldstein, *Fluid Mechanics Measurements*, 2nd edition (Taylor & Francis, London, 1996).
[2] S. A. Cha and J. D. Trolinger, *Proceedings of The International Society for Optical Engineering* (SPIE, Bellingham, WA, 1995).
[3] W. Yang, *Handbook of Flow Visualization* (Hemisphere, New York, 1989).
[4] S. V. Alekseenko, V. E. Nakoryakov, and B. G. Pokusaev, *Wave Flow of Liquid Films* (Begell House, Inc., New York, 1994).
[5] J. L. Lui, J. D. Paul, and J. P. Gollub J. Fluid Mech. **250**, 69 (1993).
[6] A. A. Knaani, R. A. Schluter, and S. G. Bankoff, Isr. Chem. Eng. J. **22**, 58 (1993).
[7] A. Oron, S. H. Davis, and S. G. Bankoff, Rev. Mod. Phys. **69**, 931 (1997).
[8] S. W. Joo, S. H. Davis, and S. G. Bankoff, J. Fluid Mech. **230**, 122 (1991).
[9] H. C. Chang Annu. Rev. Fluid Mech. **26**, 103 (1994).
[10] P. G. de Gennes Rev. Mod. Phys. **57**, 827 (1985).
[11] L. M. Hocking and M. J. Miksis J. Fluid Mech. **247**, 157 (1993).
[12] P. G. Lopez, M. J. Miksis, and S. G. Bankoff, Phys. Fluids (to be published).
[13] P. G. Lopez, M. J. Miksis, and S. G. Bankoff, J. Fluid Mech. **324**, 261 (1996).
[14] F40BL 40 Watt lamps, Phillips Lighting Co., 200 Franklin Square Dr., P.O. Box 6800, Somerset, NJ 08875.
[15] Rosco No. 48, Rosco Laboratories, Inc., 36 Bush Ave., Portchester, NY 10573.
[16] Rosco No. 10, Rosco Laboratories, Inc., 36 Bush Ave., Portchester, NY 10573.
[17] DT3851, Data Translation, 100 Locke Dr., Marlboro, MA 01752.
[18] Image-Pro Plus v. 1.3, Media Cybernetics, 8484 Georgia Av., Silver Springs, MD 20910; http://www.mediacy.com/.
[19] Fluorescein Acid Yellow 73 (Sigma CI-45350). Dyes from Sigma Chemical Co., P.O. Box 14508, St. Louis, MO 63178, except bis (phenylethynyl) anthracene from Aldrich, 1001 W. St. Paul Ave., Milwaukee, WI 53233.
[20] M. F. G. Johnson, Ph.D. thesis, Northwestern University, 1997.